

# A CFD simulation method for nozzle droplet deposition characteristics and corresponding experimental validation

Jie Yan, Jianyu Wang, Chi Lv, Songlin Wang

College of Mechanical Engineering and Automation, Liaoning University of Technology, Jinzhou, Liaoning Province, China

## Abstract

Spray booms can often tilt during operation due to factors such as uneven ground, tires deformation and crop canopy structure and height, adversely affecting droplet deposition. Therefore, it is crucial to study and understand how spray height and nozzle tilt angle affect droplet deposition to enhance the effectiveness of plant protection products (PPPs) application. The TeeJet®XR8002 nozzle was selected as the research object, and simulations and spray tests were conducted at three spray heights (0.5, 0.6, and 0.8 m) and 10 tilt angles (1°~10°). The film length and nozzle tilt

angle were used to determine the relative position of the virtual origin and the center coordinates to determine the tilt angle of the spray model. Depositional characteristics at different spray heights were analyzed using the ratio of deposition and changes in the spray height. The dense spraying effect was observed when the nozzle was tilted at spray heights of 0.5, 0.6, and 0.8 m. For spray heights of 0.8, 0.6, and 0.5 m, the maximum allowable tilt angles were 4°, 3°, and 4°, respectively, to ensure that the effect of changes in tilt angle on droplets deposition is minimized. The maximum relative errors with respect to the experimental tests for the accurate deposition ratio and deposition ratio were 3.09% and 4.64%, respectively, thus validating the reliability of the simulation results.

Correspondence: Songlin Wang, College of Mechanical Engineering and Automation, Liaoning University of Technology, No.169, Shiyong Street, Guta District, Jinzhou City, Liaoning Province, 121001 China. E-mail: wangslxss@163.com

Key words: CFD simulation; droplet deposition characteristics; nozzle tilt angle; spray height.

Contributions: all authors made a substantive intellectual contribution, read and approved the final version of the manuscript and agreed to be accountable for all aspects of the work.

Conflict of interest: the authors declare no potential conflict of interest.

Availability of data and materials: the experiments were conducted in strict alignment with the experimental concepts, and the acquired experimental data were managed in a pragmatic fashion. All data, models, and code created or utilized throughout the study are included in the submitted article. Additionally, upon request, all the data files from the tests and simulations are available.

Acknowledgements: this study was supported by General Project of Liaoning Provincial Education Department (LJKZ0606).

Received: 26 December 2023.

Accepted: 21 January 2025

©Copyright: the Author(s), 2025

Licensee PAGEPress, Italy

Journal of Agricultural Engineering 2025; LVI:1708

doi:10.4081/jae.2025.1708

This work is licensed under a Creative Commons Attribution-NonCommercial 4.0 International License (CC BY-NC 4.0).

Publisher's note: all claims expressed in this article are solely those of the authors and do not necessarily represent those of their affiliated organizations, or those of the publisher, the editors and the reviewers. Any product that may be evaluated in this article or claim that may be made by its manufacturer is not guaranteed or endorsed by the publisher.

## Introduction

Currently, 80% of domestic crops are sprayed, and the effective utilization ratio of pesticides is only approximately 30% (Yang *et al.*, 2005). Over the years, scholars have conducted relevant experimental research on droplet deposition effectiveness and drift, investigating influential factors that may reduce PPPs usage, as well as minimize environment pollution. Therefore, research on droplet deposition in spraying systems is necessary.

Song *et al.* (2006) showed that the directional angle of the fog flow and the forward speed of the spray bar influence deposition. Ding *et al.* (2020) found that spray pressure and fog flow angle affect drift, and Lv *et al.* (2011) studied the influence of wind speed and spray height on drift. Molle *et al.* (2012) reported that droplets less than 1mm in diameter exhibited the greatest losses. Losses due to evaporation represented 30~50% of the total loss; the remaining 50~70% were due to wind causing small droplets to drift outside the target zone. Due to the better atomization performance and strong anti-drift properties of liquid droplets, flat spray nozzles have always had a high usage rate in field operations, and to further improve the spraying effect of flat spray nozzles, many scholars have carried out research on them. Nuytens *et al.* (2007) found that for the same nozzle size and pressure, cone nozzles produce the finest droplet size spectrum and the highest proportion of droplets prone to drift, followed by standard flat spray nozzles and low-drift flat spray nozzles. Thompson *et al.* (2007) showed that increasing viscoelasticity of the test fluid can stabilize the thin films produced by both flat spray and hollow-cone spray nozzles, thereby shifting the break-up of the sheets to larger flow rates. Negrisoli *et al.* (2012) showed that both angled flat spray nozzles and standard flat spray nozzles were used to significantly increase crop yield at a spray rate of 125 L/ha, thereby reducing the impact of soybean rust. Foqué *et al.* (2012) reported that the use of extended range standard flat spray nozzles without air support, directed toward the crop and at a fixed spraying distance of 30 cm from the stem, usually produces the best spraying results on laurel crops. B Sayinci (2015) determined the liquid inlet and outlet velocities, discharge coefficients, and minimum

spray pressures required for atomization of nozzles of different filter types based on dimensions, shape and area measurements related to nozzle geometry. Post *et al.* (2017) measured the exit velocity of standard, pre-orifice, and air-induction flat fan nozzles, at pressure ranging from 1 to 6 bar to calculate the discharge coefficients of the corresponding nozzles. Sayinci *et al.* (2020) reported that compared with other nozzles, coarse droplet-producing nozzles at higher speeds decreased, and more uniform distributions were achieved. Kluza *et al.* (2019) established a model for predicting droplet uniformity for a flat spray nozzle based on different nozzle wear conditions.

In the case of crop sprayers, rugged road surfaces can cause the spray boom to tilt during operation, leading to changes in spray height and tilt angle, which significantly affect droplet deposition. However, few studies have focused on the relationship between the tilt angle and spray height of a flat spray nozzle and the distribution of droplet deposition. In this study, a combination of test and CFD techniques was used to obtain regions with a high percentage of droplet deposition and dense deposition for three given spray heights. The theoretical range of droplet deposition when the nozzle is not tilted is calculated according to the spraying parameters, and the influence of the tilt angle on the deposition is described according to the change of the ratio of droplet deposition in the range at the same spray height, so as to determine a reasonable range of the tilt angle of the nozzle.

## Materials and Methods

### Geometrical modeling and meshing

The computational domain model was established using Geometry, a 3D modeling software package in the Ansys 19.2 Workbench. The simulation domain was a rectangular parallelepiped with a length (X-axis) of 1.92 m, a width (Y-axis) of 1 m, and a height (Z-axis) of 0.8 m. The position of the nozzle was fixed at coordinates ( $x=0.96$  m,  $y=0.5$  m), and its height (Z-axis) was set at 0.8, 0.6, and 0.5 m respectively. To obtain the droplet distribution statistics, this study divided the bottom surface of the XOY plane into 60 regions, each measuring  $0.032$  m $\times$ 1 m, starting from the origin along the positive X-axis direction. The nozzle was situated directly above the intersection line of regions No. 30 and No. 31, as depicted in Figure 1.

Referring to the formula for determining the accurate deposition ratio proposed by Chen *et al.* (2021), this study regarded the accurate deposition range as an ellipse, as shown in Figure 2. The accurate deposition range is defined as the droplet deposition range when the nozzle is not tilted and can be calculated according to Eqs. (1) and (2). Using MATLAB 2022 software, this study screened and summed discrete points within this specified range:

$$r = h \tan(\theta_1 + \theta_2) \quad (\text{Eq. 1})$$

$$d = h \tan(\arctan \frac{a}{l_b} + \theta_2) \quad (\text{Eq. 2})$$

where  $h$  represents the spray height (m),  $r$  represents the long half-axis of the accurate range (m),  $d$  represents the short half-axis of the accurate range (m), and  $a$  and  $l_b$  are the short half-axis of the spray nozzle and the length of the liquid film, respectively (m).  $\theta_1$  is the spray half-angle ( $\theta_1=40^\circ$ ),  $\theta_2$  is the diffusion angle ( $\theta_2 = 6^\circ$ ).

The long axis of the nozzle TeeJet®XR8002 is 1.57 mm, and the short axis ( $2a$ ) is 0.51 mm, and the formula for calculating the length ( $l_b$ , mm) and thickness ( $2h_t$ , mm) of the liquid film is shown

in Eqs. (3) and (4), according to Wang *et al.* (2019).

$$l_b = 16.11p^{-0.33} \quad (\text{Eq. 3})$$

$$2h_t = 0.031p^{-0.316} \quad (\text{Eq. 4})$$

where  $p$  represents the nozzle pressure (MPa).

After confirming the fluid domain model, the fluid domain model was imported into the Integrated Computer Engineering and Manufacturing (ICEM) software for meshing. After importing, the model was built and divided into blocks so that the blocks fit the fluid domain model as well as possible. Since the fluid domain was a regular geometry and the whole meshing process did not involve point alignment, movement, the mesh quality could reach 1, and the number of meshes is 501316.

The continuous phase of the model is air. The research focuses on the influence of nozzle tilt angle and spray height on the droplet deposition, without considering the effect of crossflow, therefore, the velocity of the continuous phase is 0 m/s. Once the continuous phase stabilized, this study introduced the discrete phase, which signifies the introduction of droplets into the simulation.

The deposition ratios in different regions were calculated as follows:

$$p_i = \frac{m_i}{\sum_{i=1}^{60} m_i} \times 100\% \quad (\text{Eq. 5})$$

where  $i$  represents the region number ( $i=1,2,3,\dots,60$ ) and  $m_i$  represents the mass of liquid collected in the corresponding region.

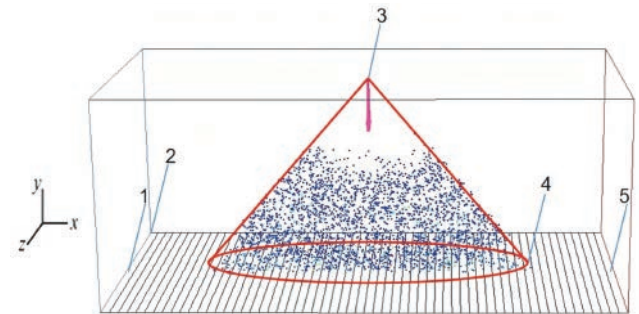


**Figure 1.** Fluid domain model. 1. Deposition region no. 1; 2. coordinate origin; 3. nozzle position; 4. accurate deposition range; 5. deposition region no. 60.

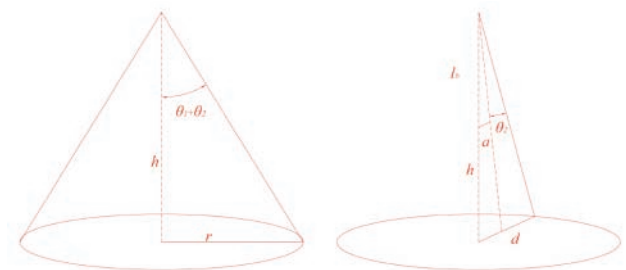


**Figure 2.** Accurate deposition range.

The distribution of droplets is an important indicator of deposition characteristics. In this study, the deposition ratio was analyzed in different regions to observe the effect of spray height on the deposition characteristics. In addition, this study studied the effect of the tilt angle by considering the elliptical spray cross-section of the flat spray nozzle and assuming the exit cross-section of the nozzle as approximately elliptical (Wang *et al.* 2019). When the nozzle was tilted, a new deposition range was created, as illustrated in Figure 3. The ratio of droplet deposition in the overlap between the tilted nozzle deposition range and the accurate deposition range is the accurate deposition ratio. A ratio closer to 1 indicates that the deposition effect at a specific tilt angle closely matches the standard situation. The formula for calculating the accurate deposition ratio is shown in Eq. (6)

$$W_n = \frac{\sum_{\substack{u \leq x \leq s \\ t < y < j}} P(x,y)}{\sum_{\substack{0.96-r \leq x \leq 0.96+r \\ 0.5-d < y < 0.5+d}} P(x,y)} \times 100\% \quad (\text{Eq. 6})$$

where  $W_n$  represents the accurate deposition ratio for different tilt angles under the same spray height ( $n=1,2,3,\dots,10^\circ$ ). Furthermore,  $u, s, t,$  and  $j$  represent the range of the droplets deposition at a certain tilt angle under the same spray height, and  $p(x,y)$  represents the mass of the droplets at the corresponding coordinates. The larger the  $W_n$  value is, the smaller the offset of the droplet under the corresponding tilt angle.

In addition, to determine the extent to which the variation between adjacent tilt angles affect the accurate deposition ratio and to determine the suitable range of tilt angles, the variation in the accurate deposition ratio between adjacent tilt angles at the same spray height  $D_n$  was used as a measure by referring to the study by Xue *et al.* (2021) on the optimum spray height:

$$D_n = |W_n - W_{n-1}| \quad (\text{Eq. 7})$$

where  $D_n$  represents the change in the deposition ratio at the corresponding tilt angle ( $n=1,2,3,\dots,10^\circ$ ). When  $n=1$ ,  $W_0$  is the accurate deposition ratio when spraying vertically. The larger the corresponding value of  $D_n$  is, the more the deposition ratio is affected by the tilt angle between  $(n-1)^\circ$  and  $n^\circ$ .

### Fluid calculation models

This simulation was a pressure-based transient simulation, considering the effect of gravity, the direction was the negative Z-axis, the gravitational acceleration was taken as  $9.81 \text{ m/s}^2$ , and the continuous phase model was adopted as the k-epsilon model, whose transport equations are shown in Eqs. (8) and (9):

$$\frac{\partial(\rho k)}{\partial t} + \frac{\partial(\rho k u_i)}{\partial x_i} = \frac{\partial}{\partial x_j} \left[ \left( \mu + \frac{\mu_t}{\sigma_k} \right) \frac{\partial k}{\partial x_j} \right] + G_k + G_b - \rho \epsilon - Y_M + S_k \quad (\text{Eq. 8})$$

$$\frac{\partial(\rho \epsilon)}{\partial t} + \frac{\partial(\rho \epsilon u_i)}{\partial x_i} = \frac{\partial}{\partial x_j} \left[ \left( \mu + \frac{\mu_t}{\sigma_\epsilon} \right) \frac{\partial \epsilon}{\partial x_j} \right] + C_{1\epsilon} \frac{\epsilon}{k} (G_k + C_{3\epsilon} G_b) - C_{2\epsilon} \rho \frac{\epsilon^2}{k} + S_\epsilon \quad (\text{Eq. 9})$$

where  $k$  is the turbulent kinetic energy ( $\text{m}^2/\text{s}^2$ ),  $\epsilon$  is the turbulent energy dissipation rate ( $\text{m}^2/\text{s}^3$ ),  $\sigma_k$  and  $\sigma_\epsilon$  are simply the turbulent Prandtl numbers for  $k$  and  $\epsilon$ , respectively;  $G_k$  represents the production of turbulence kinetic energy due to the mean velocity gradient (Pa/s),  $G_b$  is the generation of turbulence kinetic energy due to buoyancy (Pa/s);  $\mu$  is the continuous phase kinetic viscosity (Pa·s);  $\mu_t$  is the turbulent viscosity (Pa·s);  $\rho$  is the continuous phase

density ( $\text{kg}/\text{m}^3$ );  $t$  is time (s);  $u_i$  is the velocity in the  $i$ -th direction (m/s);  $Y_M$  is the effect of the pulsating expansion of compressible turbulence on the total dissipation rate (Pa/s);  $S_k$  is a user-defined term (Pa/s);  $S_\epsilon$  is a user-defined term (Pa/s<sup>2</sup>); and  $C_{1\epsilon}$ ,  $C_{2\epsilon}$ , and  $C_{3\epsilon}$  are empirical constants with values of 1.44, 1.92, and 0.09, respectively.

The discrete phase droplet equations of motion were solved according to the Euler-Lagrange method proposed by Crowe and Smoot (1979), and the discrete phase particle equations of motion are given in Eq. (10):

$$\frac{du_p}{dt} = \frac{18\mu C_D R_e}{24\rho_p d_p^2} (u - u_p) + \frac{g_x(\rho_p - \rho)}{\rho_p} + \frac{1}{2} \frac{\rho}{\rho_p} \frac{d}{dt} (u - u_p) \quad (\text{Eq. 10})$$

where  $u$  is the continuous phase velocity (m/s),  $u_p$  is the particle velocity (m/s),  $\rho_p$  is the particle density ( $\text{kg}/\text{m}^3$ ),  $d_p$  is the particle diameter (m),  $g_x$  is the gravitational acceleration ( $\text{m}/\text{s}^2$ ),  $R_e$  is the relative Reynolds number, and  $C_D$  is the coefficient of drag.

### Simulation test parameter settings

**Parameters of the discrete-phase spray source:** this study used water as the discrete-phase material with droplet as the particle type. The operating pressure of the nozzle was set to 0.3 MPa. The position of the nozzle is the virtual origin position in the solver, and the center coordinates are determined from the liquid film length and the nozzle tilt angle, as shown in Figure 4. The formula

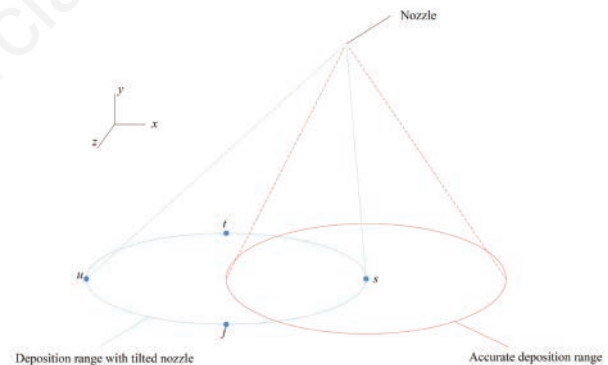


**Figure 3.** Accurate deposition range and deposition range with tilted nozzle.

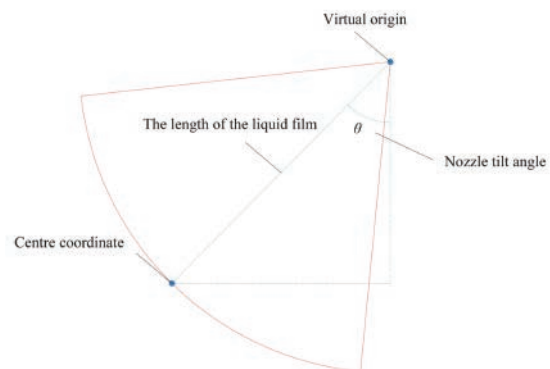


**Figure 4.** Relative position of the virtual origin to the center coordinates.

for calculating the length of the liquid film is shown in Eq. (3). The nozzle flow rate was 0.013317 kg/s under the pressure of 0.3 MPa according to Wang *et al.* (2019), with a spray half-angle of 40° and a spray diffusion angle of 6°; in addition, unsteady particle tracking and Discrete Element Method (DEM) collisions were enabled. The orifice width in the solver is the liquid film thickness, which is calculated according to Eq. (4). The number of streams selected was 2000. The changes in total droplet deposition obtained from 2500 and 3000 streams compared to 2000 streams are shown in Table 1. A greater number of streams did not necessarily have a greater impact on the data but increased the solution time more, so the number of streams was 2000 in this study.

**Boundary condition parameters:** The continuous phase inlet at  $x = -0.96$  m was set as the velocity inlet, the continuous phase outlet at face  $x = 0.96$  m was set as the velocity outlet (outlet-vent), and all other faces were wall boundaries (wall). For discrete-phase boundary conditions, the velocity inlet and velocity exit were set to Escape, the bottom face ( $Z=0$ ) was Collect (Trap), and the rest were Escape.

**Simulation parameters:** A nonstationary simulation was performed considering the effect of gravity. The simulation was run for 10 s with an iteration step of 0.05 s and a total of 200 steps. The pressure-velocity coupling mode was selected as the SIMPLE, and the default sub-relaxation factor was used. Standard initialization was selected as the initialization method.

### Droplet spraying test and equipment

To assess the reliability of the CFD model, the setup is illustrated in Figures 5 and 6. It is made up by three parts: the spraying system, the regulating devices and the collection test bench. The spraying system mainly consisted of a water tank, air compressor,

and TeeJet®XR8002 spray nozzle. Air is passed through the compressor and then through the regulator into the water tank; the water is pressurized and then passed through the pipeline to the spray nozzle for atomization, as shown in Figure 5. The regulating device mainly consists of a regulator, a manometer, a tilt angle adjustment device, and a solenoid valve. The tilt angle adjustment device is directly connected to the nozzle so that the nozzle tilt angle can be easily changed during the test. As shown in Figure 7, because pressure is one of the most important indicators of droplet size, it is necessary to control the pressure through the regulator. The collection device is composed of a “V”-type patternator with 60 regions and corresponding 60 test tubes. Each recess represents a deposition region, as shown in Figure 5 and Figure 8.

Prior to the test, the nozzle was positioned above the intersecting line of the 30th and 31st regions to ensure vertical alignment. The mass of the test tube under the “V”-type patternator was measured. The spraying parameters were as follows: pressure=0.3 MPa, nozzle flow rate=0.799 L/min (0.013317 kg/s), and spray half-angle ( $\theta_1$ ) =40°. The spray heights were 0.8, 0.6, and 0.5 m. The nozzle sprayed at all given heights with a tilt angle in the range of 0° to 10° and an interval of 1°. The pre-spraying time was 5 s each test, which makes sure the spraying was stable. After pre-spraying, immediately move the test tubes to the droplet collection position, and collect the droplets for 65 s. The droplets deposited in each region were collected into corresponding test tubes. After each test, weigh the test tube with a balance. The mass of droplet deposition in the region was expressed by corresponding tube mass difference before and after the test. Each test was repeated three times. During the tests, the air temperature was 27°C and the relative humidity was 50%.



**Figure 5.** Photographs of the test site. 1. Air compressor; 2. pressure gauge; 3. water tank; 4. timing relay; 5. regulator; 6. switch.

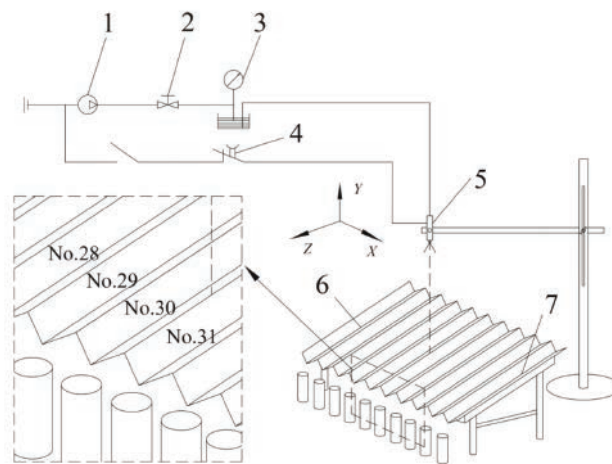


**Figure 6.** Schematic of the test setup. 1. Air compressor; 2. regulator; 3. pressure gauge; 4. timing relay; 5. nozzle; 6. no. 1 region; 7. no. 60 region.

**Table 1.** Changes in droplet deposition compared to 2000 streams.

Spray height (m) and tilt angles (°)	Number of data streams (2500)	Number of data streams (3000)
0.6 m and 10°	0.973%	1.513%
0.5 m and 8°	0.036%	0.142%
0.8 m and 6°	0.497%	0.210%

### Evaluation indicators and data processing

This paper evaluated the effect of spray height on deposition characteristics as a function of the droplet deposition in different regions and described the effect of tilt angle on deposition characteristics through the accurate deposition ratio. The number of regions covered by the radius of the accurate deposition range was calculated using Eqs. (1) and (11):

$$n = \frac{r}{0.032} \tag{Eq. 11}$$

where  $r$  is the half-length axis of the accurate deposition range (m), and  $n$  represents the number of regions covered by the half-length axis of the accurate deposition range.

According to Eqs. (1) and (11), the number of regions covered by the radius of the accurate deposition range is generally a decimal. To improve the accuracy of the test, a special method of taking integers was adopted, taking the region to the right of the nozzle (X-axis positive) as an example:

$$c = \frac{p_{[n]}}{p_{([n]+1)}} \tag{Eq. 12}$$

where  $[n]$  represents an integer to  $n$ , and  $p_{[n]}$  and  $p_{[n+1]}$  represent the masses of the droplets in the corresponding deposition region (g). The  $([n]+1)$ -th region on the right side of the nozzle is not included in the accurate deposition range if  $c < 0.5$ . Otherwise, this region is included in the accurate deposition range.

After determining the accurate deposition range on both sides of the nozzle at a certain spray height, when the nozzle was tilted, the accurate deposition ratio  $z_n$  corresponding to the tilt angle can be expressed as follows:

$$z_n = \frac{\sum_c m_i}{\sum_l m_i} \times 100\% \tag{Eq. 13}$$

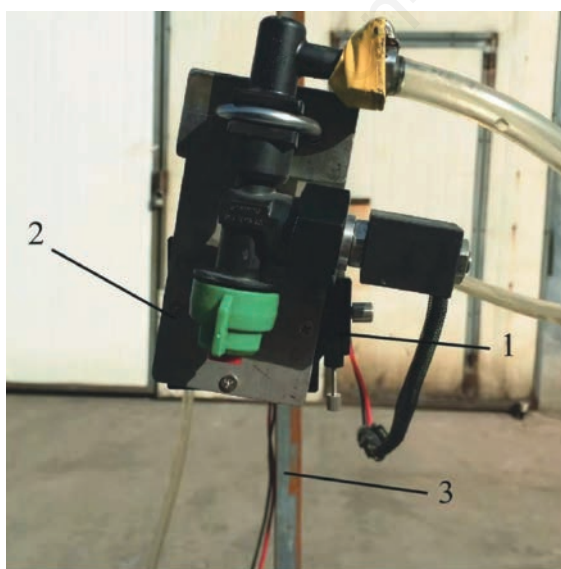


**Figure 7.** Nozzle tilt angle adjustment device. 1. Inclination-adjusting device; 2. nozzle; 3. bracket.

where  $f$  and  $l$  represent the accurate deposition range,  $c$  and  $y$  represent the deposition range at a certain tilt angle, and  $m_i$  represents the regional deposition mass. The larger the value of  $z_n$  is, the smaller the effect of the tilt angle on the deposition.



**Figure 8.** Droplet collection device. 1. Wave through; 2. test tube diagrams.



**Figure 9.** Spray pattern under different spraying conditions. **A)** Spraying height: 0.5 m - tilt angle: 1°. **B)** Spraying height: 0.6 m - tilt angle: 1°. **C)** Spraying height: 0.8m - tilt angle: 1°..

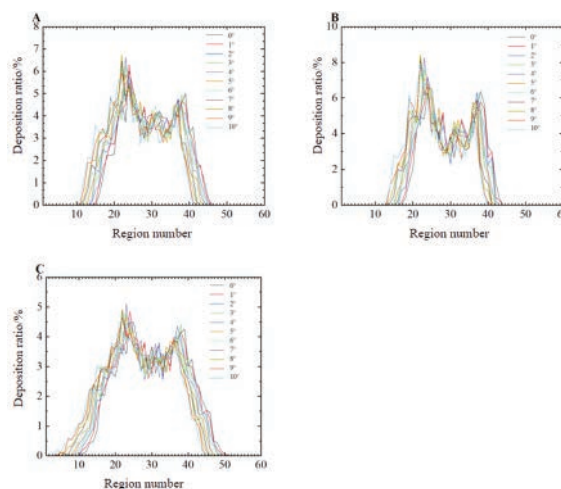


**Figure 10.** Deposition ratio at three heights: 60 cm (A); 50 cm (B); 80 cm (C).

## Results

### Numerical simulation results

In the absence of lateral winds, the discrete phase droplets were distributed in a sector with a spray half-angle of  $40^\circ$  when the nozzle tilt angle and spray height were varied. With the change of spray height and tilt angle, the deposition range changed significantly. The spray patterns under different conditions were shown in Figure 9, and the deposition ratios under different conditions were shown in Figure 10. As shown in Figure 10, the deposition rate in the deposition area were generally large, which was in line with the characteristics of flat spray nozzles, but the bimodal pattern in the middle area showed that the simulation model needed to be further optimized.

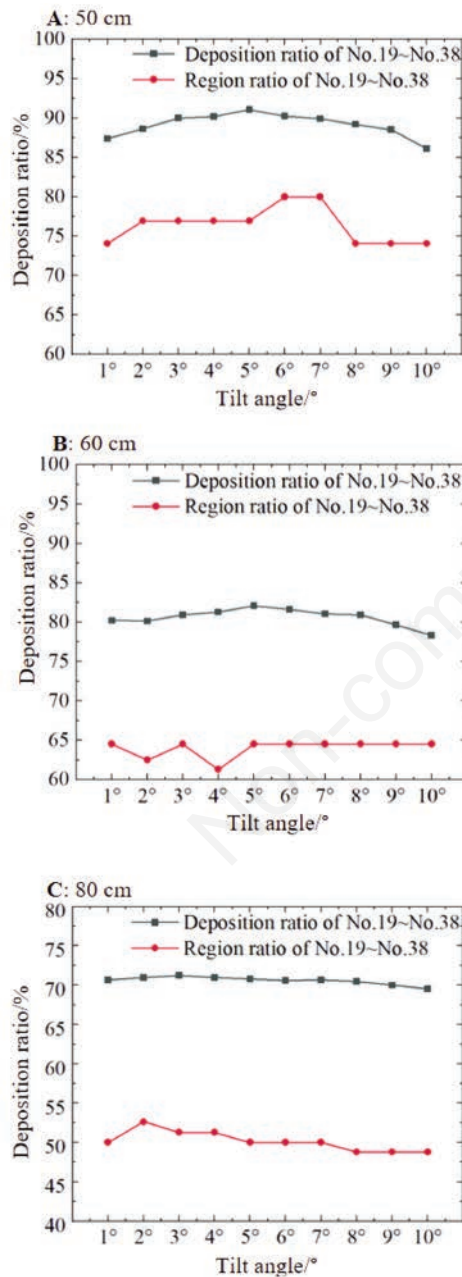


**Figure 11.** Deposition ratio at three heights: 60 cm (A); 50 cm (B); 80 cm (C).

### Deposition ratios at different spray heights

The deposition ratios at different tilt angles for spray heights of 0.8, 0.6, and 0.5 m are shown in Figure 10. As the spray height increased, there was a corresponding increase in deposition range, allowing droplets to cover more regions. At spray heights of 0.8, 0.6, and 0.5 m, as the tilt angle increased, there was an increase in droplet deposition towards the nozzle tilt direction, while deposition in the opposite direction decreased. Although changes in the nozzle's tilt angle can affect droplet distribution, the average ratios of deposition within the range spanning from No.19 to No.38 were 70.59%, 80.62%, and 89.03% at spray heights of 0.8, 0.6, and 0.5 m, respectively. Deposition ranges at different tilt angles may vary, and the range ratios of regions 19–38 may also be different. However, under all the given parameters, the deposition ratios of regions 19–38 were still higher compared with their range ratios. This suggests a denser distribution of droplets within this No.19 to No.38 region, as depicted in Figure 11. According to Eq. (1), as the total spraying amount remains constant, increasing the spray height results in greater coverage of the nozzle with droplets, while the ratio of deposition in the region from No. 19 to No. 38 decreases. Moreover, collisions between droplets are influenced, causing changes in droplet size distribution. The resistance experienced by droplets during descent is associated with deposition velocity and atmospheric turbulence; smaller droplets face greater resistance.

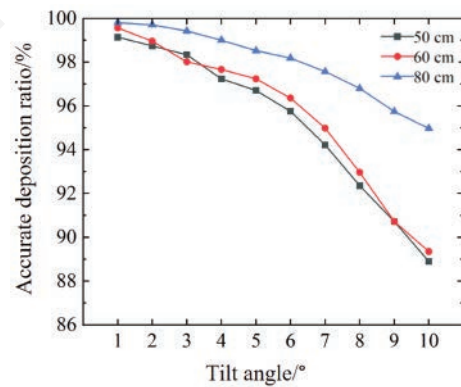


**Figure 12.** Accurate deposition ratios at different heights.

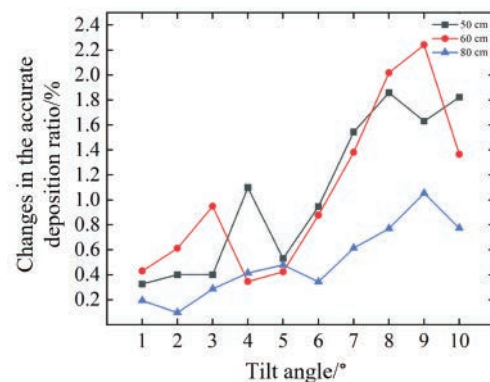


**Figure 13.** Changes in the accurate deposition ratio between adjacent tilt angles.

Consequently, even at very low droplet velocities, some droplets settle further away (Løfstrøm *et al.*, 2013). Therefore, the ratio of droplet deposition in the region from No.19 to No.38 was notably lower than the deposition ratio between 0.5 m and 0.6 m at a spray height of 0.8 m. Droplet size influences deposition distribution (Gil *et al.*, 2014). To this end, Jia *et al.* (2018) showed that under the same conditions, the particle size of droplet increased consid-

erably when the spray height was between 0.3 m and 0.5 m, while the growth trend of particle size was slower when the spray height was between 0.5 m and 0.7 m. Therefore, the ratio of droplet deposition in regions No.19~38 was similarly affected by the tilt angle at spray heights of 0.5 m vs 0.6 m but significantly different from that at 0.8 m.

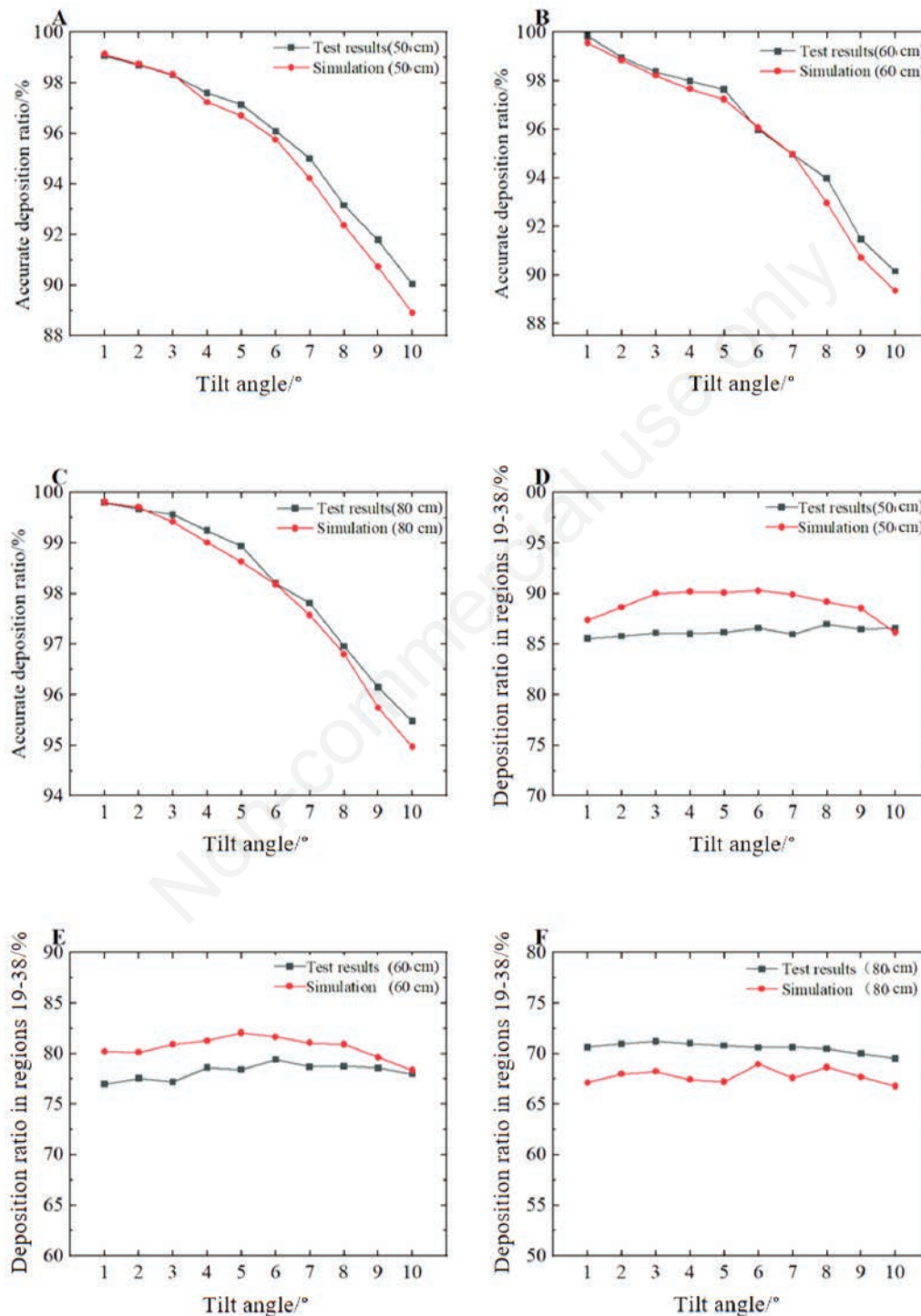


Figure 14. Comparison graphs of the simulation and test results.

## Effect of tilt angle on deposition characteristics

As shown in Figure 10, as the nozzle was tilted, the overall deposition range moved in the direction of the nozzle tilt. To further assess the effect of tilt on deposition characteristics and determine the maximum allowable tilt angle for the TeeJet®XR8002 nozzle at different spray heights, this study examined the accurate deposition ratio under various conditions, as shown in Figure 12. The changes in the deposition ratio  $D_n$  are shown in Figure 13.

At spray heights of 0.8, 0.6, and 0.5 m, the accurate deposition ratio gradually decreased with increasing tilt angle. The average values of the change in the accurate deposition ratio between adjacent tilt angles  $D_n$  for spray heights of 0.8, 0.6, and 0.5 m were 0.503%, 1.064%, and 1.056%, respectively. As shown in Figures 12 and 13, at a spray height of 0.8 m, the largest accurate deposition ratio at all tilt angles with the smallest change in deposition ratio between adjacent tilt angles was observed. However, at this spray height, when the tilt angle reached 4°, 5°, and 7°, the corresponding change in accurate deposition ratios  $D_4$ ,  $D_5$ , and  $D_7$  were 0.41%, 0.47%, and 0.61%, respectively. Although the change in the accurate deposition ratio  $D_7$  exceeded the mean value for the first time at 7°, the  $D_n$  values before the tilt angle of 4° were significantly smaller than the mean value. The change in the accurate deposition ratio  $D_4$  when the tilt angle reached 4° was significantly greater than the change in  $D$  at all previous tilt angles, with 4° being the maximum permissible tilt angle under a spray height of 0.8 m. Similarly, at a spray height of 0.6 m, although the change in the accurate deposition ratio at 7° ( $D_7$ ) was 1.38%, exceeding the average value for the first time, the change in the accurate deposition ratio between adjacent tilt angles at 3° ( $D_3$ ) was 0.95%, which is significantly greater than the change in  $D$  at all previous tilt angles. Therefore, 3° was considered the maximum permissible tilt angle at a spray height of 0.6 m. When the spray height was 0.5 m, the change in the accurate deposition ratio between adjacent tilt angles at 4° was 1.098%, which is greater than the average value of the change in the accurate deposition ratio at the same spray height. All the  $D$  values before 4° were small and changed steadily. Therefore, 4° was considered the maximum permissible tilt angle under a spray height of 0.5 m.

## Discussion

In the simulation, deposition ratio in regions of No.19~No.38 was used to describe the influence of the spray height on the deposition characteristics of the TeeJet®XR8002 nozzle, and the accurate deposition ratio and the change between neighboring tilt angles were used to describe the influence of the spray angle on the deposition characteristics. Comparison graphs of the simulation and test results for these metrics are shown in Figure 14.

The test data show that at all three spray heights, the deposition ratio of the TeeJet®XR8002 nozzle decreased with increasing tilt angle. The accurate deposition ratio was greater at 4°, 3°, and 4° at spray heights of 0.8, 0.6, and 0.5 m, respectively, and the changes in the accurate deposition ratio before that were small and relatively stable. Thus, 4°, 3°, and 4° were considered the maximum permissible tilt angles at 0.8, 0.6, and 0.5 m, respectively, which are consistent with the simulation results. The average ratios of deposition within the range spanning from No.19 to No.38 at 0.8, 0.6, and 0.5 m in the test results were 67.77%, 78.21%, and 86.21%, respectively. These results are close to the corresponding simulation results of 70.59%, 80.62%, and 89.03%, respectively, with relative errors of <5%. The presence of side winds in the test environment affected the test results, deviating from the theoretical values.

However, the maximum relative error of the deposition ratio in the No.19~No.38 regions was 4.64% (when the spray height was 0.5 m and the tilt angle was 4°), and the maximum relative error of the accurate deposition ratio was 3.09% (when the spray height was 0.6 m and the tilt angle was 10°), which is consistent with the simulation results and further illustrates the accuracy of the simulation results.

## Conclusions

This study focused on the TeeJet®XR8002 flat spray nozzle and utilized the CFD discrete phase model to simulate droplet deposition characteristics at spray heights of 0.5, 0.6, and 0.8 m. The results were validated experimentally, yielding the following conclusions:

The best spraying effect was observed when the nozzle was deflected within the range of 0.384 m on the left side to 0.256 m on the right side at spray heights of 0.5, 0.6, and 0.8 m.

To ensure high deposition efficiency, the maximum permissible tilt angles under spray heights of 0.8, 0.6, and 0.5 m were found to be 4°, 3°, and 4°, respectively. When the spray height was 0.5 m, the deposition ratio was most affected by the tilt angle, and when the spray height was 0.8 m, the deposition ratio was least affected by the tilt angle.

The deposition characteristics of a single nozzle can serve as a foundation for future research on the deposition patterns of spray boom. This exploration could aid in refining the design of automated spraying control systems, ultimately enhancing droplet deposition efficiency and precision in agricultural spraying applications.

## References

- Chen, S., Zhan, Y., Lan, Y., Yan, Y., Qian, S., Chen, W., Chen, L. 2021. Influence of crosswind on droplet drift of flat-fan nozzle in aviation plant protection UAV. *J. South China Agr. Univ.* 42:89-98.
- Crowe, C.T., Smoot, L.D. 1979. Multicomponent conservation equations. pulverized-coal combustion and gasification: theory and applications for continuous flow processes. In: Smoot, L.D., Pratt, D.T. (eds) *Pulverized-coal combustion and gasification*. Springer, Boston, pp. 15-54
- Ding, S., Xue, X., Dong, X., Gu, W., Zhou, Q. 2020. Effects of spraying parameters on droplet deposition performance. *Trans. Chin. Soc. Agr. Mach.* 51:308-15.
- Foqué, D., Pieters, J.G., Nuyttens, D. 2012. Spray deposition and distribution in abay laurel crop as affected by nozzle type, air assistance and spray direction when using vertical spray booms. *Crop Prot.* 41:77-87.
- Gil, E., Balsari, P., Gallart, M., Llorens, J., Marucco, P., Andersen, P.G., Fàbregas, X., Llop, J. 2014. Determination of drift potential of different flat fan nozzles on a boom sprayer using a test bench. *Crop Prot.* 56:58-68.
- Jia, W., Li, X., Zhou, H., Gong, C., Ou, M. 2018. Analysis and experimental study on the working process of the seedling clamping mechanism of cam. *J. Agr. Mech. Res.* 40:10-20.
- Kluza, P.A., Kuna-Broniowska, I., Parafiniuk, S. 2019. Modeling and prediction of the uniformity of spray liquid coverage from flat fan spray nozzles. *Sustainability (Basel)* 11:6716.
- Lv, X., Fu, X., Song, J., He, X. 2011. Influence of spray operating parameters on spray drift. *Trans. Chin. Soc. Agr. Mach.* 42:59-63.
- Løfstrøm, P., Bruus, M., Andersen, H.V., Kjær, C., Nuyttens, D.,

- Astrup, P. 2013. The oml-spraydrift model for predicting pesticide drift and deposition from ground boom sprayers. *J. Pestic. Sci.* 38:129-38.
- Molle, B., Tomas, S., Hendawi, M., Granier, J. 2012. Evaporation and wind drift losses during sprinkler irrigation influenced by droplet size distribution. *Irrig. Drain.* 61:240-250.
- Negrisoni, M.M., Raetano, C.G., Souza, D.M.D., Santos e Souza F.M., Bernardes, L.M., Del Bem Junior, L., et al. 2019. Performance of new flat fan nozzle design in spray deposition, penetration and control of soybean rust. *Eur. J. Plant Pathol.* 155:755-767.
- Nuyttens, D., Baetens, K., De Schampheleire, M., Sonck, B. 2007. Effect of nozzle type, size and pressure on spray droplet characteristics. *Biosyst. Eng.* 97:333-345.
- Post, S.L., Roten, R.L., Connell, R.J. 2017. Discharge coefficients of flat-fan nozzles. *Trans. ASABE* 60:347-351.
- Sayinci, B. 2015. Effect of strainer type, spray pressure, and orifice size on the discharge coefficient of standard flat-fan nozzles. *Turk. J. Agric. For.* 39:692-704.
- Sayinci, B., Demir, B., Acik, N. 2020. Comparison of spray nozzles in terms of spray coverage and drop distribution uniformity at low volume. *Turk. J. Agric. For.* 44: 262-270.
- Song, J., He, X., Yang, X. 2006. Influence of nozzle orientation on spray deposit. *Trans. Chin. Soc. Agr. Eng.* 22:96-99.
- Thompson, J.C., Rothstein, J.P. 2007. The atomization of viscoelastic fluids in flat-fan and hollow-cone spray nozzles. *J. Non-Newtonian Fluid Mech.* 147:11-22.
- Wang, S., Dou, H., Zhao, X., Wang, X., Zhao, C. 2019. Modeling liquid sheet and droplet distribution of flat-fan nozzle. *Int. Agr. Eng. J.* 28:88-99.
- Xue, S., Xi, X., Lan, Z., Wen, R., Ma, X. 2021. Longitudinal drift behaviors and spatial transport efficiency for spraying pesticide droplets. *Int. J. Heat Mass. Transfer.* 177: 21516.
- Yang, X., Yan, H., Zhou, H. 2005. Experimental study on fan spray nozzle. *J. Chin. Agr. Mech.* 1:39-42.

Non-commercial use only